STM observation of pit formation and evolution during the epitaxial growth of Si on Si(001) surface*

Xu Mao-Jie(徐茂杰)[a], Jeyanthinath Mayandi[b], Wang Xue-Sen(王学森)[b], Jia Jin-Feng(贾金锋)[a], Xue Qi-Kun(薛其坤)[c], and Dou Xiao-Ming(窦晓鸣)[a,d,†]

[a] *Institute of Optical Engineering, Shanghai Jiao Tong University, Shanghai* 200240, *China*

[b] *Department of Physics, National University of Singapore, Lower Kent Ridge Road,* 119260, *Singapore*

[c] *Department of Physics, Tsinghua University, Beijing* 100084, *China*

[d] *School of Optical-Electrical and Computer Engineering, University of Shanghai for Science and Technology, Shanghai* 200093, *China*

(Received 9 February 2010; revised manuscript received 13 May 2010)

Pit formation and surface morphological evolution in Si(001) homoepitaxy are investigated by using scanning tunneling microscopy. Anti-phase boundary is found to give rise to initial generation of pits bound by bunched D_B steps. The terraces break up and are reduced to a critical nucleus size with pit formation. Due to anisotropic kinetics, a downhill bias diffusion current, which is larger along the dimer rows through the centre area of the terrace than through the area close to the edge, leads to the prevalence of pits bound by {101} facets. Subsequent annealing results in a shape transition from {101}-faceted pits to multi-faceted pits.

Keywords: pit, facet, homoepitaxy, Si(001)

PACC: 6116P, 6855

1. Introduction

Si(001)-2×1 surface has attracted considerable interest due to its relatively simple structure and technological importance.[1−20] Great efforts focus on the construction of nano-meter sized structures on the surface aiming at the establishment of semiconductor nanotechnologies. Kinetic instabilities in homoepitaxy are actively exploited to produce highly regular patterns on crystalline surfaces.[1] Depending on Si deposition condition and Si(001) wafer miscut angle, various patterns are formed, such as ripples,[2] step fingers,[3] mounds,[4] triangles, and ridges.[5] The morphological instabilities are attributed to the anisotropic kinetics inherent to the (2×1)-dimer reconstruction of Si(001) surface. Anisotropic diffusion of adatoms on the terraces and across the step edges,[6] and much higher adatom incorporation probability at the end of dimer rows than at the side[7] are the key ingredients for the spatial pattern formation.

Surface defects such as vacancies, steps, and anti-phase boundaries (APBs), often play an essentially important role in the control of growth process and fabrication of desired nanostructures. Si(001)-$2 \times n$ surface with vacancy line structure from Ni contamination was used for spontaneous fabrication of nanowire arrays.[8] The flow of steps in epitaxial film facilitates smooth growth by suppressing the island nucleation.[9] Kissing sites occur at the end of APBs on Si(001) surface and are of great importance for evaluating the feasibility to use the surface for a specific device or process.[10] In this study, we show the pit formation on the base of APB combining with anistropic kinetics provides an interesting means for tailoring surface structures.

2. Experimental

Our experiments were conducted in an ultrahigh vacuum (UHV) system ($\sim 5 \times 10^{-9}$ Pa) equipped with scanning tunneling microscopy (STM), low-energy electron diffraction (LEED), and Auger electron spectroscopy (AES). Si(001) wafers were degassed below 600 °C overnight with a basic pressure better than 3×10^{-8} Pa, and then slowly heated up to 900 °C

*Project supported by the grants from the National University of Singapore (R-144-000-069-101) and the SERC of Singapore (R-144-000-088-305).

†Corresponding author. E-mail: xmdou@sjtu.edu.cn; mjxu@sjtu.edu.cn

© 2010 Chinese Physical Society and IOP Publishing Ltd

prior to quick flashing to 1200 °C. The Si(001) wafer miscut angle is smaller than 0.15° and the average of terrace width is larger than 50 nm. Si deposition was performed using an electron bombardment source at a deposition rate of 0.5∼6 ML/min. All STM images were recorded at room temperature with a tunneling current of ∼ 0.2 nA.

3. Results and discussion

Figure 1 shows the well-faceted pits after the growth of 27-ML Si on Si(001) surface. We measured statistically the slopes of the facets surrounding the initially formed pits [see Fig. 1(a)] and found that the facets have the miller index of {113} facet. An STM image of typical pit bound by {113} facets and a line scan through the pit are shown in Fig. 1(b).

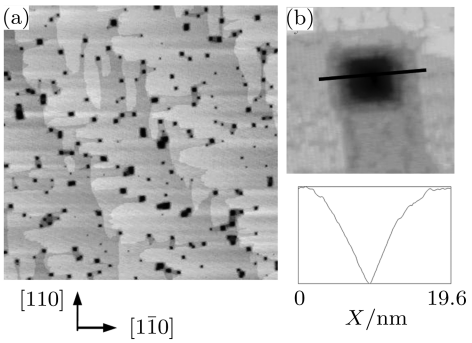


Fig. 1. (a) STM image (500 ×500 nm^2) of 27-ML epitaxial Si film with initially formed pits on Si(001) surface grown at T_S = 650 °C, F = 2.7 ML/min. (b) Top: STM image (26 ×26 nm^2) of a well-faceted pit, bottom: a linear scan through the pit showing the slope of facets.

A model structure of {113}-faceted pit forming on the base of APBs is shown as Fig. 2. Due to the 2×1 dimer reconstruction of Si(001) surface, APBs occur when two independently nucleated adatom islands with internal misaligned dimer rows meet [see Fig. 2(a)].[11] An APB1 forms when two adatom islands meet at S_A step, and APB2 forms when two adatoms islands meet at S_B step. The APB2 is observed to be the preferential site for Si island nucleation,[12] whereas APB1 is found to lead to formation of two out-of-phase D_B steps [Figs. 2(b) and 2(c)].[13] Since the lifting of 2×1 reconstruction and the annihilation of two out-of-phase D_B steps require much high activation energy, the pit formation is closely associated with APB1.

The appearance of {113} facets was observed in epitaxial Si layers on SiO_2-patterned Si(001) surfaces and related to growth kinetics.[14] A step-related kinetic pathway for bunching of D_B steps was proposed to lead to {113} facets.[15] Both rebonded and nonrebonded D_B steps are found to be energetically stable according to the theoretical study.[15] The rebonded D_B step reduces dangling bond density at the expense of strain energy, whereas nonrebonded D_B step releases the strain energy with high dangling bond density. The competition between dangling bond reduction and strain energy release leads to the alternating bunching of rebonded and nonrebonded D_B steps. The facets formed by the alternating bunching has the miller indices of {113}. Thus, we propose the facets surrounding the pits are formed by alternating bunching of rebonded and nonrebonded D_B steps [see Figs. 2(d) and 2(e)].

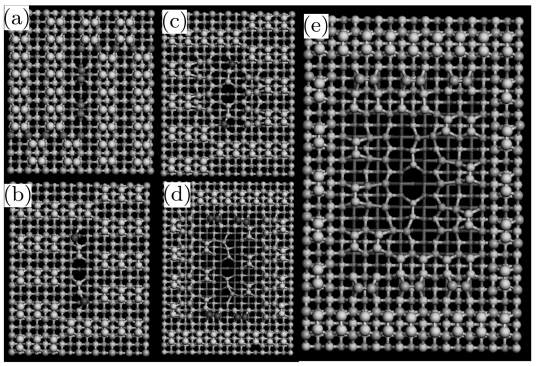


Fig. 2. Model structure showing pit formation on the base of APB (large ball representing the top layer Si atom, smaller ball the lower layer atom) (a) APB structure; (b) two out-of-phase nonrebonded D_B steps with two adatoms to saturate the dangle bonds, (c) rebonded D_B steps, (d) pit bound by bunching of rebonded D_B step on nonrebonded D_B step, and (e) pit bound by bunching of nonrebonded D_B step on rebonded D_B step.

Figure 3 shows pit formation and surface morphological evolution during the growth of Si on Si(001) at a substrate temperature of 650 °C and a flux of 2.7 ML/min. In the initial growth stage, Si adatom islands nucleate on the large terraces and lead to APB formation when the dimer rows in neighbouring islands are misaligned. On the base of APBs, pits bound by bunching of D_B steps are formed leading to the terrace breaking [see Figs. 1(a) and 3(a)]. When the top terrace size is reduced to be smaller than the critical base size for second layer island nucleation,[16] APB cannot emerge to lead to pit formation since only one island nucleates on the terrace. In a previous study, a typical critical size of ∼ 650 dimers for second layer island nucleation was obtained when depositing Si on Si(001) surface at growth temperature of 650 °C

and flux smaller than 2.0 ML/min.[17] The equilibrium adatom concentration, external deposition, and adatom incorporation at island edge contribute to the incoming Si flux for determining the critical nucleus size. We found a critical nucleus size larger than 10000 dimers when the equilibrium adatom concentration is not dominant and the island edge effect cannot be neglected.

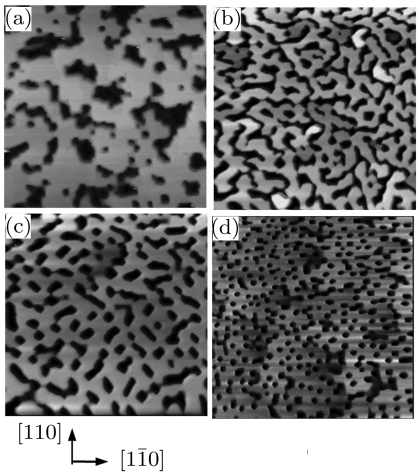


Fig. 3. STM images of Si(001) surfaces after Si deposition at $T_S = 650$ °C, $F = 2.7$ ML/min for (a) 30 min; (b) 90 min; (c) 150 min; (d) 250 min. Scan areas and black to white gray scales are (a) 600×600 nm^2, and 9 nm; (b) 2000×2000 nm^2, and 35 nm; (c) 2000×2000 nm^2, and 45 nm; (d) 3725×3725 nm^2, and 66 nm.

Kinked steps are formed when the pits coalesce [see Figs. 1(a) and 3(a)]. No Ehrlich–Schwoebel (ES) barriers that suppress downward interlayer transport of adatoms are reported so far for either S_A or S_B steps on Si(001) surface. D_B step, however, is predicted to be associated with a relatively high ES barrier.[15] Because the diffusion barrier for adatoms across kinked steps is smaller than the D_B steps, an additional downhill bias current is generated with the kinked step formation and the critical size for second layer island nucleation becomes larger because of the reduced incoming flux. Due to the diffusion anisotropy and higher probability for adatom sticking to the end of dimer row than the side, the bias current along the dimer row through the centre area of top terrace is larger than that through the area close to the edge, which leads to the prevalence of {101}-faceted pits [see Figs. 3(b) and 3(c)]. With increasing downhill bias current, top terraces merge and the average pit top size enlarges through pit coalescing and annihilating. The correlation of top terraces plays an important role in surface roughening and leads to increasing critical thickness for epitaxial growth.

The average top size of pit and the average distance between nearest-neighbour pits are found to be $\sim$13500 nm^2 and $\sim$140 nm for 405-ML thick film [see Fig. 3(c)]. The average pit top size and spacing increase to $\sim$21500 nm^2 and $\sim$170 nm for 675-ML thick film [see Fig. 3(d)]. By controlling Si growth condition and Si wafer miscut angle, the surface with desired pit size and spacing can be grown.

Subsequent annealing of 675-ML thick film at above 650 °C results in a shape transition from {101}-faceted pit to multi-faceted pit. Figure 4(a) shows a large area STM image of surface morphology after annealing. Figures 4(b) and 4(c) show the STM images of a typical {101}-faceted pit, and a multi-faceted pit. The $\{11n\}$ facets appear and expand with {101} facets shrinking. {001} facets emerge at the bottom of multi-faceted pits. The surface free energy governs the pit shape transition and $\{11n\}$ facet formation during annealing. Recently, the pits with $\{11n\}$ facet walls are observed for the growth of Si on pit-patterned Si(001).[21]

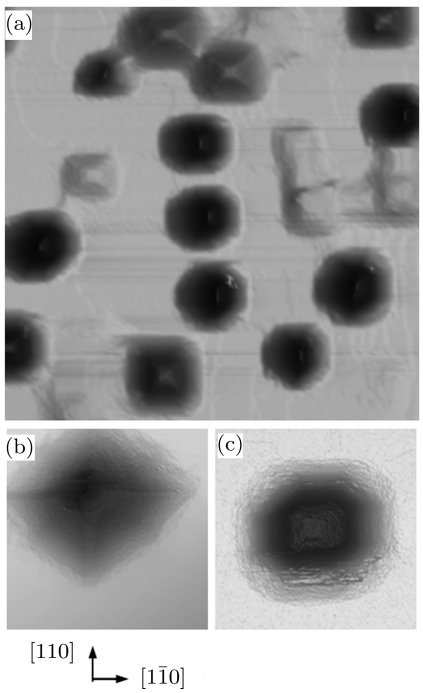


Fig. 4. (a) STM image (1000×1000 nm^2) of 675-ML epitaxial Si film grown on Si(001) surface at $T_s = 650$ °C, $F = 2.7$ ML/min and annealed at above 650 °C, (b) STM image (200×200 nm^2) of a typical {101}-faceted pit, (c) STM image (220×220 nm^2) of a typical multi-faceted pit.

4. Conclusions

In conclusion, the pit formation on the base of APB and anisotropic kinetics inherent to the

2×1 dimer reconstruction of Si(001) surface induce patterning on the surface. Initially, pit bound by {113} facets is formed, which is attributed to the alternating bunching of rebonded and nonrebonded D_B steps. {101}-faceted pits prevail in consequent epitaxy. During annealing, {101}-faceted pit evolves into multi-faceted pit to lower the surface free energy. By optimizing growth condition and substrate miscut angle, nanopatterned Si(001) surface with desirable pit size, shape and spacing can be fabricated, which can be used as template for growing quantum nanostructures such as negative Ge islands,[22] inverse Ge dome, and quantum dot molecules.[23]

References

[1] Politi P, Grenet G, Marty A, Ponchet A and Villain J 2000 *Phys. Rep.* **324** 271

[2] Wingerden J, Halen E C, Werner K, Scholte P and Tuinstra F 1996 *Surf. Sci.* **352–354** 641

[3] Wu F, Jaloviar S G, Savage D E and Lagally M G 1993 *Phys. Rev. Lett.* **71** 4190

[4] Lee N E, Cahill D G and Greene J E 1996 *Phys. Rev.* B **53** 7876

[5] Schelling C, Springholz G and Schäffler F 1999 *Phys. Rev. Lett.* **83** 995

[6] Mo Y W and Lagally M G 1991 *Surf. Sci.* **248** 313

[7] Mo Y W, Swartzentruber B S, Kariotis R, Webb M B and Lagally M G 1989 *Phys. Rev. Lett.* 63 2393

[8] Li J L, Liang X J, Jia J F, Liu X, Wang J Z, Wang E G and Xue Q K 2001 *Appl. Phys. Lett.* **79** 2826

[9] Neave J H, Dobson P J, Joyce B A and Zhang J 1985 *Appl. Phys. Lett.* **47** 100

[10] Swartzentruber B S, Mo Y W and Lagally M G 1991 *Appl. Phys. Lett.* **58** 822

[11] Hamers R J, Köhler V K and Demuth J E 1990 *J. Vac. Sci. Technol.* A **8** 195

[12] Bronikowski M J, Wang Y and Hamers R J 1993 *Phys. Rev.* B **48** 12361

[13] Zandvliet H J W, Zoethout E, Wulfhekel W and Poelsema B 2001 *Surf. Sci.* **482** 391

[14] Hirayama H, Hiroi M and Ide T 1993 *Phys. Rev.* B **48** 17331

[15] Oshiyama A 1995 *Phys. Rev. Lett.* **74** 130

[16] Tersoff J, Denier van der Gon A W and Tromp R M 1994 *Phys. Rev. Lett.* **72** 266

[17] Theis W and Tromp R M 1996 *Phys. Rev. Lett.* **76** 2770

[18] Huang Y and Zhu X Y 2004 *Chin. Phys.* **13** 725

[19] Xu T B, Zhu P R, Zhou J S, Li D Q, Ren T Q, Zhao Q T, Liu X D and Liu J T 1995 *Acta Phys. Sin.* (Overseas Edn.) **4** 118

[20] Wang C Q, Jia Y, Ma B X, Wang S Y, Qin Z, Wang F, Wu L K and Li X J 2005 *Acta Phys. Sin.* **54** 4313 (in Chinese)

[21] Sanduijav B, Matei D, Chen G, Schäffler F, Bauer G and Springholz G 2008 *Thin Solid Films* **517** 293

[22] Akazawa H 2008 *Appl. Phys. Express* **1** 071402

[23] Songmuang R, Kiravittaya S and Schmidt O G 2003 *Appl. Phys. Lett.* **82** 2892